# Probing the Nanoscale Viscoelasticity of Intracellular Fluids in Living Cells

Gernot Guigas, Claudia Kalla, and Matthias Weiss
Cellular Biophysics Group, German Cancer Research Center, Heidelberg, Germany

ABSTRACT We have used fluorescence correlation spectroscopy to determine the anomalous diffusion properties of fluorescently tagged gold beads in the cytoplasm and the nucleus of living cells. From the extracted mean-square displacement $\nu(\tau) \sim \tau^{\alpha}$, we have determined the complex shear modulus $G(\omega) \sim \omega^{\alpha}$ for both compartments. Without treatment, all tested cell lines showed a strong viscoelastic behavior of the cytoplasm and the nucleoplasm, highlighting the crowdedness of these intracellular fluids. We also found a similar viscoelastic response in frog egg extract, which tended toward a solely viscous behavior upon dilution. When cells were osmotically stressed, the diffusion became less anomalous and the viscoelastic response changed. In particular, the anomality changed from $\alpha \approx 0.55$ to $\alpha \approx 0.66$, which indicates that the Zimm model for polymer solutions under varying solvent conditions is a good empirical description of the material properties of the cytoplasm and the nucleoplasm. Since osmotic stress may eventually trigger cell death, we propose, on the basis of our observations, that intracellular fluids are maintained in a state similar to crowded polymer solutions under good solvent conditions to keep the cell viable.

## INTRODUCTION

The cytoplasm of virtually all living cells, from bacteria to mammals, is a highly crowded and structured fluid in which up to 40% of the total mass is contributed by dissolved macromolecules (1). In other words, 1 ml cytoplasm may contain ~400 mg of proteins, lipids, nucleic acids, and sugars. In the nucleus, crowding is further enhanced by the hierarchically organized chromatin, which penetrates the interchromatin space (2). The effects of crowding on the chemistry of life, e.g., the change of reaction equilibria due to excluded volume, have been discussed in some detail (3–6). Equally important, crowding has been shown to affect the diffusional properties of proteins in the cytoplasm: as a rather mild effect, the reduction of the diffusion coefficient as compared to an aqueous solution has been reported repeatedly (7–12); recently, a more dramatic effect, namely the qualitative change of the diffusional motion toward anomalous subdiffusion, has been reported for nanoscale tracer particles in crowded solutions like the cytoplasm (13–15) and the nucleoplasm (16). A hallmark of anomalous subdiffusion is the nonlinear growth of the mean-square displacement (MSD) of a particle in time, i.e., $\nu(t) \sim t^{\alpha}$ with $\alpha < 1$ ($\alpha = 1$ for normal diffusion). It is noteworthy that anomalous subdiffusion has not only been observed in the context of crowded solutions but also for the movement of lipids on model membranes (17) and integral membrane proteins on intracellular membranes (18). Although anomalous subdiffusion may at first glance appear as an academic curiosity of nature, its occurrence has been shown to strongly influence kinetic rates (19), the formation of spatiotemporal patterns (20,21), and the time course of enzymatic reactions (22,23).

Although determining the MSD yields important insights into the diffusive properties of proteins for further use in modeling, the information encoded in the MSD also allows one to draw conclusions about the properties of the fluid in which the Brownian motion took place (24). One particularly interesting quantity in this respect is the complex shear modulus $G(\omega) = G'(\omega) + iG''(\omega)$, which measures the viscous ($G''$) and elastic ($G'$) moduli when exciting a fluid with an oscillatory shear strain of frequency $\omega$. Whereas a material like rubber is almost purely elastic ($G'' = 0$), water is an almost purely viscous fluid ($G' = 0$) with vanishing restoring forces upon shear deformation. More complex fluids are, in general, viscoelastic ($G', G'' \neq 0$), i.e., depending on the frequency of the imposed strain, a more or less elastic response is obtained. On macroscopic scales, $G(\omega)$ for bulk solutions is frequently determined with a torsion pendulum (25), whereas for thin films the perturbations of an acoustic surface wave may be utilized (26). To quantify $G(\omega)$ on the micro- and nanoscales, Mason and Weitz have proposed an elegant scheme that essentially relies on the Laplace-transformed MSD (24), which can be measured with fluorescence methods, e.g., fluorescence correlation spectroscopy (FCS) or single-particle tracking (SPT). Although SPT has already been utilized to assess the viscoelasticity of the cytoplasm, nucleoplasm (27,28), and actin solutions (29,30), its limited time resolution and the use of large beads with diameters of ~100 nm have been a disadvantage. The same limitations are typically encountered when using magnetic tweezers (31). So far, SPT and magnetic-bead rheology have been used mainly in the context of untreated cells. Yet, bearing in mind the aforementioned connection between crowding and anomalous subdiffusion, osmotically stressing cells can be expected to alter the degree of crowding and thus change the viscoelastic properties of the cytoplasm and the nucleoplasm.

Here, we have used FCS to investigate the diffusional behavior of inert gold nanoparticles in the cytoplasm and

*Submitted October 10, 2006, and accepted for publication February 26, 2007.*

Address reprint requests to Matthias Weiss, Cellular Biophysics Group, B085, German Cancer Research Ctr., Im Neuenheimer Feld 580, D-69120 Heidelberg, Germany. E-mail: m.weiss@dkfz.de.

Editor: Gaudenz Danuser.



0006-3495/07/07/316/08 $2.00

doi: 10.1529/biophysj.106.099267

nucleoplasm under various stress conditions. In addition, we tested the properties of (diluted) frog egg extract. In all cases, we have observed strong anomalous subdiffusion with varying degrees of anomality. From the MSD, we have obtained the complex shear modulus, which reflects the viscoelastic properties of the cytoplasm and nucleoplasm on the nanoscale. Although both fluids appear remarkably viscoelastic in untreated cells, osmotic stress (e.g., addition of sucrose to the medium) reduced the elastic response and softened the degree of anomality of the diffusion. In fact, the frequency dependence of the shear modulus is well described by the Zimm model for polymer solutions with varying solvent conditions. In support of this view, qualitatively similar observations were obtained for artificially crowded solutions using different solvents.

## MATERIALS AND METHODS

### Cell culture and microscopy

Wild-type HeLa and HepG2 cells were grown at 37°C in DMEM (+10% fetal calf serum, +1% penicillin-streptomycin). THLE cells were grown at 37°C in bronchial epithelial cell basal medium (Clonetics, San Diego, CA). Colloidal gold conjugates (diameter 5 nm, tagged with AlexaFluor488 and streptavidin, saturated with BSA; Molecular Probes, Eugene, OR) were microinjected using an AIS2 microinjection system (Cellbiology Trading, Hamburg, Germany) based on an Eppendorf Femtojet injection system. Injection tips were pulled with a P97 tip puller (Sutter Instruments, Novato, CA) from borosilicate thin-wall capillaries with filament (length, 100 mm; OD, 1.2 mm; ID, 0.94 mm). TexasRed dextran (10,000 mol wt; Molecular Probes) was used as a coinjection marker. Gold colloids were incubated with D-Biotin (244.31 mol wt; Invitrogen, Carlsbad, CA) before injection to saturate the streptavidin tags. FCS measurements were performed with a Leica SP2-TCS confocal-laser scanning microscope equipped with a water immersion objective (HCX PL APO 63 × 1.2W CORR) and an FCS unit (both, Leica Microsystems, Mannheim, Germany). Samples were illuminated with a 488-nm Ar laser, the fluorescence was detected using a bandpass 500–530 nm and a pinhole size of 1 Airy unit. The sample and the microscope were held at 37°C by a climate chamber (Life Imaging Services, Reinach, Switzerland). During the measurement, cells were kept in MEM (without phenol red) + 25 mM Hepes. To create osmotic stress, sucrose, raffinose, NaCl, or urea was added to the medium 45 min before starting the measurement, with final concentrations as given in the main text. Egg extract from *Xenopus laevis* was a kind gift of T. Surrey (EMBL Heidelberg, Heidelberg, Germany). Before making FCS measurements, we determined the initial protein concentration of the extract to be $c_0 = 12.8$ mg/ml, in agreement with previous reports (32).

### Fluorescence correlation spectroscopy and data analysis

In FCS, a laser beam with Gaussian intensity profile is parked at the locus of interest and the fluorescence signal $F(t)$ from the confocal volume (~1 fl) is recorded. Due to the diffusion of labeled particles into and out of the confocal volume, $F(t)$ is only constant on average and shows stationary fluctuations $f(t)$, i.e., $F(t) = \langle F\rangle + f(t)$ (brackets denote a temporal average). By calculating the autocorrelation $C(\tau) = \langle f(t) \times f(t+\tau)\rangle/\langle F\rangle^2$ from the experimental data and fitting it with appropriate theoretical expressions, one can determine the properties of the particles' diffusion. For a more extensive introduction, we refer the reader to Rigler (33).

For diffusion in bulk solution, the appropriate theoretical expression reads, in general,

$$C(\tau) = \frac{A}{(1+w(\tau))\sqrt{1+w(\tau)/S^2}}, \qquad (1)$$

with $w(\tau) = \tau/\tau_D$ for normal diffusion. Here, $S$ denotes the unavoidable elongation of the confocal volume along the optical axis, and $\tau_D = r_0^2/(4D)$ is the mean dwell time of a particle in the confocal volume. The latter is determined by the diffusion coefficient $D$ and the beam waist $r_0$. The prefactor $A$ is inversely proportional to the mean number of particles in the confocal volume and also includes the photophysics of the fluorophore. Typically, a fraction $f_T$ of the excited fluorophores enters a nonfluorescent triplet state of lifetime $\tau_T$, which is considered by taking $A \approx (1 + f_T \exp(-\tau/\tau_T))$. For anomalous subdiffusion, the MSD follows the scaling $v(t) \sim t^\alpha$ and, thus, $w(\tau) = (\tau/\tau_s)^\alpha$ (13), where $\tau_s$ denotes the mean dwell time in the confocal volume for anomalous subdiffusion. As mentioned in the main text, subdiffusion is generically a transient phenomenon and normal diffusion is restored beyond a certain timescale. To account for this, we have used in this study an empiric expression that accounts for this transition: $w(\tau) = \tau/\tau_D + (\tau/\tau_s)^\alpha$, where typically $\tau_D > 10$ ms and $\tau_s < 1$ ms.

We have verified that for free diffusion in water, the autocorrelation function of the fluorescence was well fitted by Eq. 1 when assuming normal diffusion ($\tau_D \approx 125$ $\mu$s), i.e., our analysis is not affected by perturbations of the confocal volume (see discussions in Weiss et al. (18) and Hess et al. (34)). Fitting was performed with XMGRACE (see http://plasma-gate.weizmann.ac.il/Grace). Using the Einstein-Stokes equation $D = k_BT/(6\pi\eta R)$ ($k_BT$, thermal energy; $R$, particle radius; $\eta$, viscosity of water) the theoretical diffusion coefficient for the gold bead in water is given by $D \approx 90$ $\mu$m$^2$/s. Via $r_0^2 = 4D\tau_D$ we thus obtained $r_0 \approx 210$ nm.

### Calculation of the complex shear modulus

We follow the strategy of Mason and Weitz (24) to extract $G(\omega)$ from the MSD $v(t)$, i.e.,

$$G(\omega) = \frac{k_BT}{i\,\pi\,\omega\,R\tilde{v}(i\omega)}, \qquad (2)$$

where $k_BT$ is the thermal energy, $R$ is the radius of the diffusing particle, and $\tilde{v}(i\omega)$ is the Laplace-transformed MSD with an imaginary argument. Using $w(\tau) = \tau/\tau_D + (\tau/\tau_s)^\alpha$ in Eq. 1, and determining the MSD according to $v(\tau) = r_0^2 \times w(\tau)$, one obtains $\tilde{v}(i\omega) = a\Gamma(\alpha+1)/(i\omega)^{\alpha+1} - b/\omega^2$, with prefactors $a = r_0^2/\tau_s^\alpha$, $b = r_0^2/\tau_D$, and $\Gamma(x)$ the gamma function. Inserting this expression into Eq. 2 and using $i^\alpha = \exp(-i\pi\alpha/2)$ yields the real and imaginary part of $G(\omega)$ in a straightforward way. In particular, for $\tau_D \to \infty$ we find an asymptotic scaling $|G(\omega)| \sim (\tau_s\omega)^\alpha$.

We emphasize that the extraction of the complex shear modulus via the Laplace transformation is a rather robust approach. We have artificially introduced exponential deviations from the simple scaling of $v(\tau)$ at the beginning and end of the experimentally determined MSD curves and hardly observed changes in $G(\omega)$ more than half an order of magnitude away from the boundaries of the corresponding frequency range.

## RESULTS

To probe the diffusional behavior of nanosized particles in intracellular fluids under various conditions, and thus to determine the associated material properties of these fluids, we have injected fluorescently tagged gold nanoparticles (diameter 5 nm) into the cytoplasm of living cells (see Methods). After injection into the cytoplasm, the gold nanoparticles were dispersed over the whole cellular interior (including the nucleus) within a few minutes. Fluorescent dextran was used as a coinjection marker to identify cells

into which minute amounts of gold beads had been injected. About 2–3 h after injection, the diffusional properties of the gold nanoparticles were measured by means of FCS. Although the diffusion of the gold beads in water as determined by FCS was most consistent with normal diffusion of a single component in a three-dimensional medium (Fig. 1), we found strongly anomalous subdiffusion in the cytoplasm and nucleus of all tested cell lines (HeLa, HepG2, and THLE). Representative examples are shown in Fig. 1. Without treatment, measurements on all cell types showed an anomality of $\alpha \approx 0.53$ and a typical residence time of $\tau_s \sim 300$ $\mu$s of the gold nanoparticles in the confocal volume (see Tables 1 and 2) when measuring in the cytoplasm or the nucleus; for times $>85$ ms, normal diffusion was recovered. The latter observation is consistent with previous proposals that anomalous subdiffusion due to obstruction/crowding should be a transient rather than an asymptotic phenomenon (13,35,36).

Inspecting the determined anomalities $\alpha$ in more detail, slight differences between the cytoplasm and nucleoplasm and between the various cell types were observed. Consistently, $\alpha$ was larger in the nucleus than in the cytoplasm. Since lower values for $\alpha$ are a criterion for increased crowding (13), this indicates that the interior of the nucleus is slightly less crowded than the cytoplasm. THLE cells (which are derived from healthy liver tissue) consistently showed a somewhat lower residence time $\tau_s$ in the cytoplasm and the nucleus with respect to HepG2 cells (derived from cancerous liver tissue). It is therefore tempting to assume that cancerous cells (like HepG2) have in general a tendency for an increased crowding with respect to a comparable noncancerous cell line (like THLE).

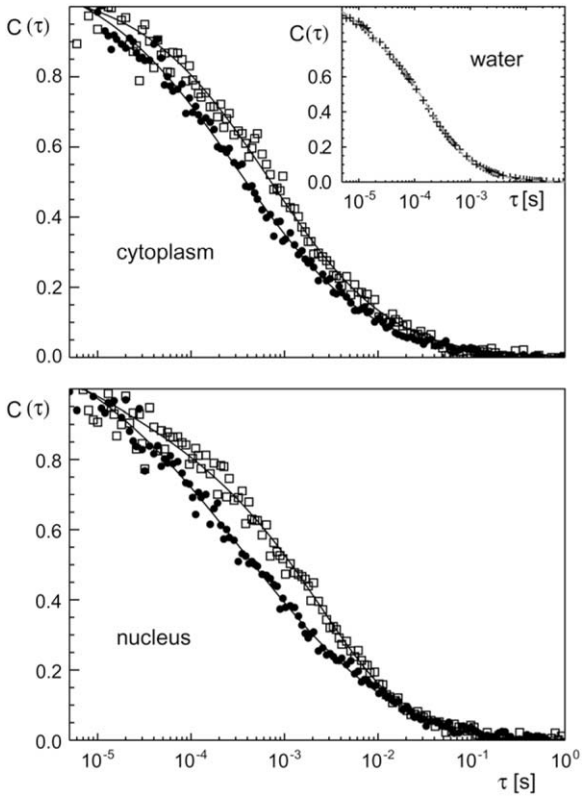


FIGURE 1 Representative FCS curves $C(\tau)$ of gold particles diffusing in the cytoplasm and the nucleus of untreated HeLa cells (*solid circles*). A clear change is seen in both cases when cells were osmotically stressed by adding 500 mM sucrose to the medium (*open squares*). (*Inset*) The autocorrelation decay of the fluorescent gold particles in water (*crosses*) is well described by normal diffusion. Solid lines are best fits with Eq. 1.

**TABLE 1 Summary of results in cytoplasm**

| Cell type | Treatment (mM) | $\alpha$ | $\tau_s$ ($\mu$s) | $\tau_D$ (ms) | $G'$(100 Hz) (Pa) | $G''$(100 Hz) (Pa) |
|---|---|---|---|---|---|---|
| HeLa | None | 0.51 | 271 | 91 | 1.00 | 1.06 |
| HeLa | sucrose, 300 | 0.56 | 853 | 89 | 1.41 | 1.78 |
| HeLa | Sucrose, 500 | 0.66 | 954 | 92 | 0.94 | 1.64 |
| HeLa | Sucrose, 1000 | 0.68 | 1933 | 89 | 1.32 | 2.52 |
| HeLa | raffinose 500 | 0.65 | 1520 | 92 | 0.31 | 0.51 |
| HeLa | NaCl, 250 | 0.52 | 742 | 88 | 1.57 | 1.74 |
| HeLa | NaCl, 500 | 0.67 | 689 | 89 | 0.73 | 1.30 |
| THLE | None | 0.48 | 329 | 89 | 1.28 | 1.24 |
| THLE | Sucrose, 500 | 0.60 | 1164 | 90 | 1.41 | 2.02 |
| HepG2 | None | 0.52 | 767 | 88 | 1.60 | 1.78 |
| HepG2 | Sucrose, 500 | 0.60 | 962 | 87 | 1.26 | 1.81 |

We next set out to determine the rheological properties of the cytoplasm and nucleoplasm. Since the decay of the autocorrelation curve $C(\tau)$ in FCS measurements is essentially determined by the behavior of the MSD $v(t)$, we extracted the smooth part of $v(t)$ from all measured FCS curves (see Methods). The average extracted MSD is shown in Fig. 2. Under the assumption that the monitored particle is spherical (like our gold beads), the MSD can yield the complex shear modulus $G(\omega) = G'(\omega) + iG''(\omega)$ of the surrounding fluid (24) (see Methods). Whereas the real part describes the elastic behavior, the imaginary part reflects the viscous modulus. Water as an almost purely viscous fluid of viscosity $\eta$ would thus be characterized by $G(\omega) = i\omega\eta$.

Converting the MSD into the complex shear modulus resulted typically in curves like the examples in Fig. 3. Whereas for low frequencies ($\omega < 1$ Hz) the cytoplasm and the nucleoplasm are governed by the viscous modulus, a strong elastic component arises for higher frequencies. Elastic and

**TABLE 2 Summary of results in HeLa cells, nucleoplasm**

| Cell type | Treatment (mM) | $\alpha$ | $\tau_s$ ($\mu$s) | $\tau_D$ (ms) | $G'$(100 Hz) (Pa) | $G''$(100 Hz) (Pa) |
|---|---|---|---|---|---|---|
| HeLa | None | 0.56 | 162 | 93 | 0.57 | 0.70 |
| HeLa | Sucrose, 300 | 0.55 | 1827 | 87 | 2.18 | 2.71 |
| HeLa | Sucrose, 500 | 0.63 | 1799 | 90 | 1.60 | 2.55 |
| HeLa | Sucrose, 1000 | 0.69 | 2021 | 89 | 1.30 | 2.58 |
| HeLa | Raffinose 500 | 0.65 | 2387 | 93 | 0.41 | 0.68 |
| HeLa | NaCl, 250 | 0.51 | 932 | 90 | 1.83 | 1.98 |
| HeLa | NaCl, 500 | 0.70 | 655 | 91 | 0.59 | 1.18 |
| THLE | None | 0.53 | 273 | 93 | 0.90 | 1.01 |
| THLE | Sucrose, 500 | 0.68 | 940 | 88 | 0.84 | 1.57 |
| HepG2 | None | 0.58 | 502 | 91 | 0.96 | 1.28 |
| HepG2 | Sucrose, 500 | 0.53 | 1840 | 86 | 2.33 | 2.74 |

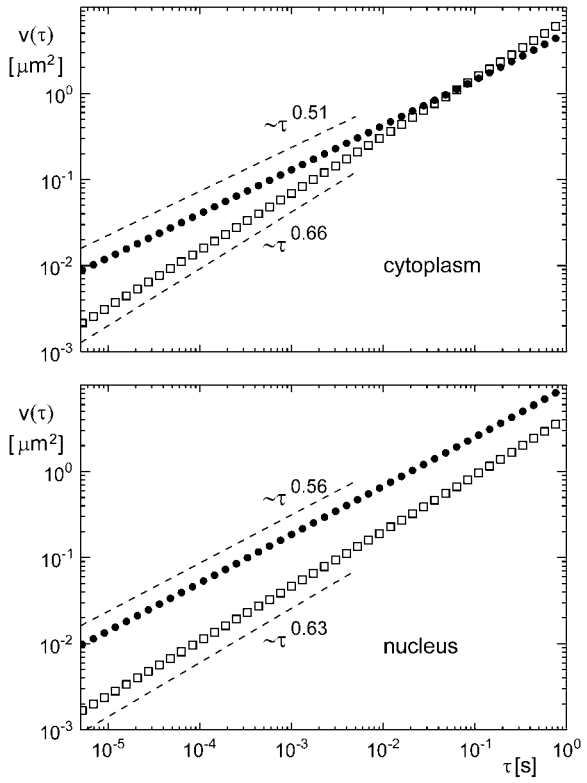


FIGURE 2 Average MSD $v(\tau)$ as obtained by fitting FCS curves with Eq. 1 (cf. Tables 1 and 2). Solid circles correspond to untreated HeLa cells, and open squares to osmotically stressed cells. The power-law increase $v(\tau) \sim \tau^{\alpha}(\alpha < 1)$ is highlighted by dashed lines.

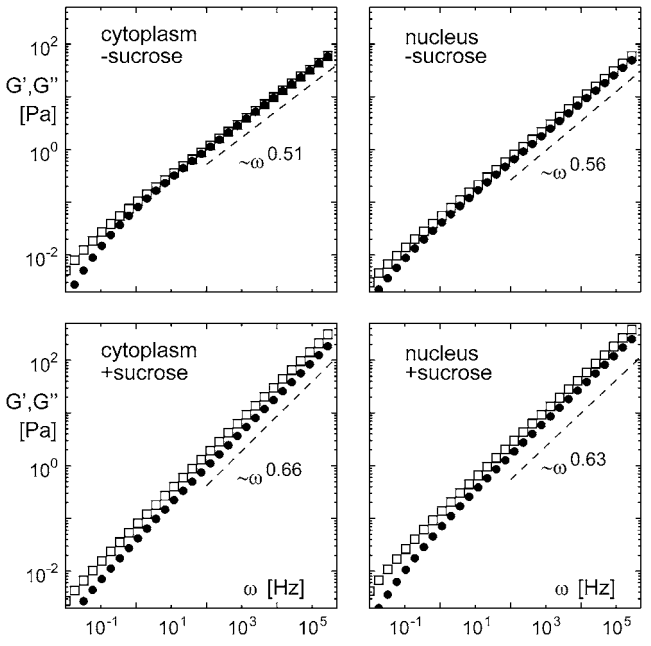


FIGURE 3 Average real (elastic) and imaginary (viscous) parts of the complex shear modulus ($G'(\omega)$ (*solid circles*) and $G''(\omega)$ (*open squares*), respectively) in the cytoplasm and nucleoplasm of HeLa cells (cf. Tables 1 and 2). The power-law increase, $G(\omega) \sim \omega^{\alpha}$, is highlighted by dashed lines.

viscous contributions are of the same order of magnitude for frequencies above $\omega \approx 1$ kHz. At $\omega \approx 10$ Hz, the real and imaginary parts of $G(\omega)$ have a typical value of ~0.3 Pa, which compares favorably with previous measurements on concentrated/crowded actin solutions (30). Notably, in accordance with the observed anomalous subdiffusion, the shear modulus shows a power-law increase $G(\omega) \sim \omega^{\alpha}$, which indicates a power-law distribution of relaxation times in the respective fluid (37). In other words, the fluid may be represented by a number of interconnected Maxwell elements (spring-dashpot in series) with a broad distribution of elastic and viscous parameters, hence enforcing a power-law distribution of relaxation times.

How can we rationalize these observations from the molecular view and explain the value $\alpha \approx 0.53$? Due to the strong crowding, macromolecules (e.g., proteins and DNA) fill the intracellular space quite densely and therefore are prone to polymeric entanglement and unspecific binding (binding energies of the order of thermal energy). Movement of a tracer particle in this environment requires unentangling, reptation, dissociation, and/or the circumvention of obstacles. All of these actions have local relaxation timescales that may differ greatly and thus lead to a power-law spectrum of relaxation times. The Zimm model for polymer solutions is a particular realization of a complex fluid with a broad spectrum of relaxation times, which is reflected by the following scaling of the complex shear modulus (38):

$$G(\omega) = B\begin{cases} (\tau_R\omega)^{5/9} & \text{good solvent} \\ (\tau_R\omega)^{2/3} & \theta - \text{solvent} \end{cases}, \qquad (3)$$

with $B \approx 1$ and $\tau_R = \eta R_g^3/(2k_BT)$. Here, $\eta$ denotes the pure solvent viscosity and $R_g$ is the radius of gyration of the polymers. Comparing the measured value $\alpha \approx 0.53$ with Eq. 3 yields a surprisingly good agreement with the Zimm model under good solvent conditions. Assuming that the cytoplasm and the nucleoplasm in untreated cells are indeed well described by Eq. 3, we can also predict the distribution of residence times $p(\tau_s)$. Since the mass $m$ of a Zimm polymer is proportional to the number of monomers $N$, and the radius of gyration is given by $R_g \sim N^{3/5}$, we expect $\tau_R \sim R_g^3 \sim m^{9/5}$. Neglecting the crossover to normal diffusion for large times, i.e., assuming that anomalous subdiffusion is also the asymptotic mode of motion, we obtain (cf. Methods) $G(\omega) \sim (\tau_s\omega)^{\alpha}$ and thus $\tau_s \sim \tau_R \sim m^{9/5}$. Since the distribution of masses in the cytoplasm is roughly exponential (13), we hence predict $p(\tau_s) \sim \exp(-\lambda\tau_s)/\tau_s^{4/5}$, i.e., for large residence times, ultimately an exponential decay of $p(\tau_s)$ should be observed. This prediction is in fairly good agreement with the experimental data for untreated cells (Fig. 4 *a*), which support the applicability of Eq. 3 as a heuristic description for intracellular fluids.

A striking prediction from Eq. 3 is a change in scaling of the shear modulus when solvent conditions become worse (i.e., going from a good solvent to a $\theta$-solvent). A reduction

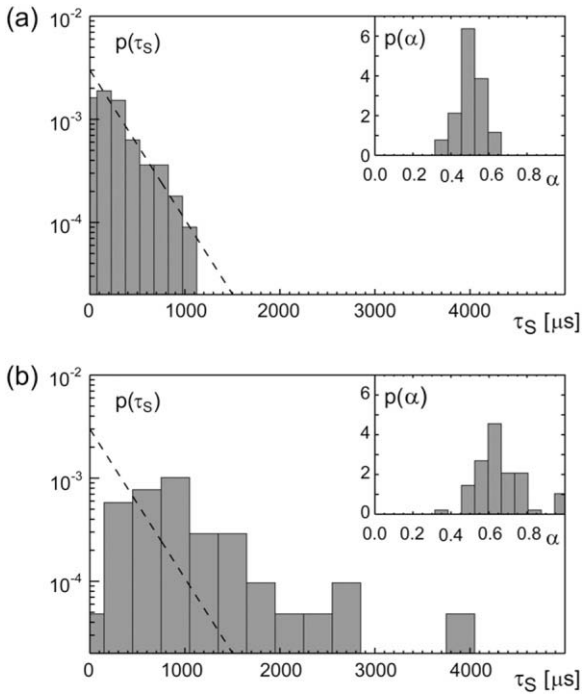


FIGURE 4 (*a*) The distribution of residence times $p(\tau_s)$ resembles the previously reported exponential distribution of masses in the cytoplasm (*dashed line*). (*b*) Upon introduction of osmotic stress, the distribution broadens and approaches a more uniform distribution. (*Insets*) The distribution of anomalities $\alpha$ is roughly Gaussian and a shift of the mean $\alpha$ is clearly visible. For better comparison, the axes have been given the same scaling.

of the available solvent due to osmotic stress (i.e., an increased crowding) should therefore affect the anomalous subdiffusion as well as the shear modulus and the distribution $p(\tau_s)$, both for the cytoplasm and the nucleoplasm. To test this prediction, we stressed cells after microinjection by adding 1), sucrose, 2), raffinose, 3), NaCl, or 4), urea to the medium and performed FCS measurements 45 min after adding the stress agent. Sucrose, raffinose, and NaCl were expected to actually induce osmotic stress, whereas urea, because it is also incorporated into the cells, was expected to have only a mild effect (if any).

Indeed, as an effect of hyperosmotic stress (using sucrose, raffinose, or NaCl), we observed a significant change in the character of the diffusion and the associated characteristic timescales. A representative FCS curve is shown in Fig. 1; the associated MSD and $G(\omega)$ are shown in Figs. 2 and 3, respectively. Interestingly, osmotic stress with up to 300–500 mM sucrose did not induce apoptosis but cells were able to grow and divide normally after changing the medium. Since higher concentrations induced apoptosis much more frequently, we concentrated on high, but nonapoptotic, conditions. Under these conditions, the diffusion became up to threefold slower in the cytoplasm and up to eightfold slower in the nucleus (indicated by an increased dwell time $\tau_s$ (cf. Tables 1 and 2)). The anomality $\alpha$ increased from $\alpha \approx 0.53$ (untreated) to $\alpha \approx 0.66$ (stressed), i.e., the diffusion became less anomalous in stressed cells. Adding urea hardly affected any of the parameters found for the cytoplasm of untreated cells, but did affect the parameters for the nucleus: the diffusion time $\tau_s$ was not strongly increased, yet the anomality was relaxed in a strength similar to that found with sucrose, raffinose, or NaCl (data not shown).

Although increased dwell time, i.e., a slower diffusion, was anticipated, the reduction of the anomality is surprising when you consider that reducing the amount of solvent water increases crowding and further ''stiffens'' the fluid. However, comparing the experimental findings for the shear modulus to Eq. 3 yields a surprisingly good agreement: the shear modulus changed its scaling to a somewhat larger exponent when the solvent became worse, and the elastic contribution decreased with respect to the viscous modulus (cf. Tables 1 and 2). An intuitive picture of the underlying dynamics in a polymer solution is the partial collapse of individual polymers, which reduces the degree of entanglement and the associated restoring forces. Changing solvent conditions in the heterogeneous intracellular fluids may also lead to a partial disentanglement and aggregation/collapse of protein complexes, i.e., more aqueous voids emerge; thereby the long-range restoring forces within the crowded fluids are reduced. Since a partial collapse/aggregation changes the distribution of the radii of gyration $R_g$, also a change in $p(\tau_s)$ was anticipated. As can be seen from Fig. 4 *b*, the distribution of residence times in the confocal volume showed not only a considerable increase in the mean dwell time, but also a broadening of the entire distribution toward a more uniform appearance.

To explore the viscoelastic behavior of crowded biofluids under more controlled conditions, we performed FCS experiments with (diluted) egg extract from *Xenopus laevis* (Methods). For the undiluted extract, we observed a degree of anomality $\alpha \approx 0.52$ similar to our results for the cytoplasm/nucleus of untreated mammalian cells. Upon dilution, the value of $\alpha$ increased toward unity, whereas the mean dwell time $\tau_s$ subsided (Fig. 5 *a* and Table 3). As expected from the Zimm theory (which was worked out for dilute polymer solutions), $\alpha$ increased only slowly upon diluting the extract, i.e., the features of a dilute polymer solution were only slowly replaced by water-like behavior. This indicates a broad range for the applicability of Eq. 3 for (intracellular) biofluids and highlights that their complexity is not a mere excluded-volume effect. Crowding in these fluids rather seems to also take into account the lateral (attractive) interactions of proteins. As anticipated from the change in $\alpha$, we also observed a decreasing ratio $G'/G''$ when diluting the extract (Fig. 5 *b*), i.e., a more water-like behavior with only a viscous contribution emerged.

To further examine the changes in a viscoelastic fluid under varying solvent conditions, we monitored the diffusion of gold beads in aqueous solutions containing 100 mg/ml unlabeled dextran (60–90 kDa, Acros Organics, Geel, Belgium). For solvents, we used pure water and a water/ethanol mixture

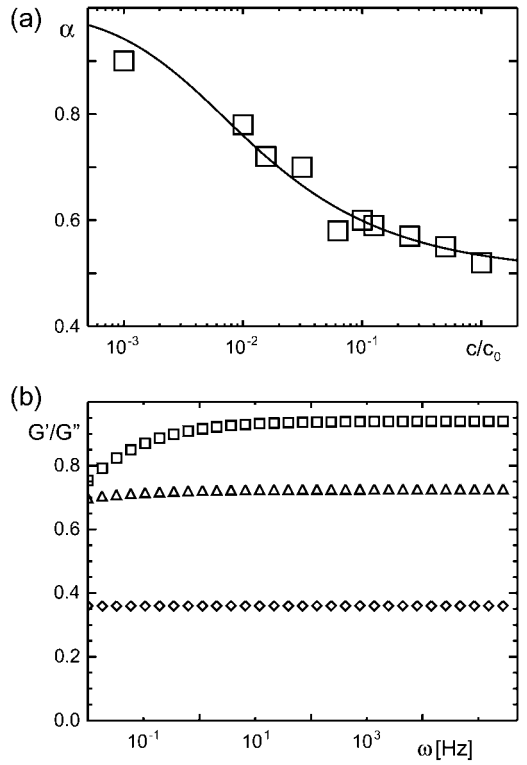


FIGURE 5 (*a*) The degree of anomality $\alpha$ measured in *Xenopus* egg extracts (initial concentration $c_0$) tends to unity upon dilution. The full line is a guide to the eye. (*b*) The ratio between elastic and viscous modulus tends toward zero upon diluting the extract. $c/c_0 = 100\%$, 10%, and 1% for squares, diamonds, and triangles, respectively.

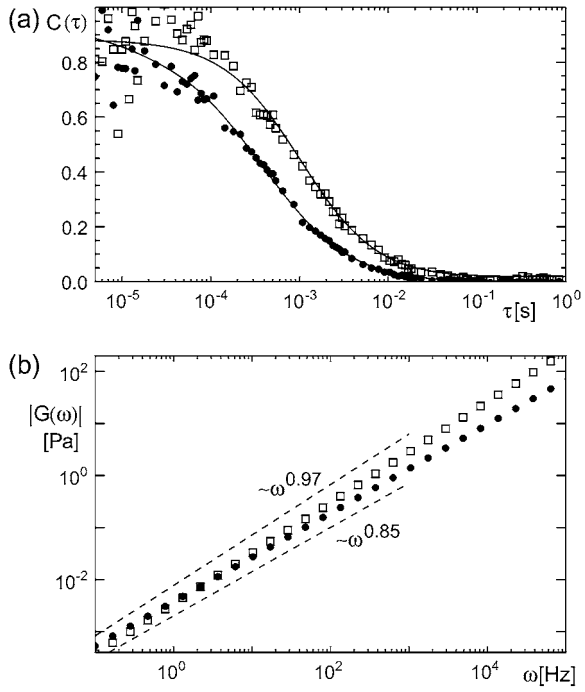


FIGURE 6 (*a*) Representative FCS curves $C(\tau)$ of gold particles diffusing in a crowded dextran solution (100 g/l) based on different solvents (*solid symbols*, pure water; *open symbols*, 60% water, 40% ethanol). A clear change in the diffusional behavior is visible. (*b*) Corresponding average modulus of the complex shear modulus ($|G(w)|$) as derived from FCS measurements. A clear change in the scaling from $\alpha = 0.85$ to $\alpha = 0.97$ is observed when changing the solvent from water to a water/ethanol mixture.

(60:40), since ethanol was expected to deteriorate the solvent conditions. As shown in Fig. 6, a strong change in the anomalous subdiffusion (as quantified by FCS) and the scaling of the shear modulus was observed when the water/ethanol solvent was used. On average, water yielded $\alpha = 0.85$, $\tau_s = 380\ \mu$s, in agreement with previous reports (13,14), whereas water/ethanol resulted in $\alpha = 0.97$, $\tau_s = 960\ \mu$s. Similar results were also found for other dextran concentrations (data not shown). We therefore conclude, in addition, that the viscoelasticity of artificially crowded solutions is altered when the solvent is improved, which is highlighted by a decrease of the exponent $\alpha$. Although we have a good qualitative agreement with the findings on intracellular fluids, Eq. 3 was not a good quantitative description here. Most likely, the utilized (almost monodisperse and low-weight) dextran did not equip the crowded fluid with enough degrees of freedom to actually reach the fully developed broad range of relaxation times that underlies Eq. 3. At this point, we would like to note also that adding even minute amounts of ethanol to the egg extract leads to massive flocculation, making FCS measurements meaningless. Nonetheless, this very observation supports indirectly our above reasoning that a change in solvent due to osmotic stress may lead to a (partial) protein collapse and/or aggregation, thus leading to a change in $\alpha$ that agrees with Eq. 3.

**TABLE 3 Summary of results in (diluted) *Xenopus* egg extract**

| Concentration | $\alpha$ | $\tau_s$ ($\mu$s) | $\tau_D$ (ms) | $G'$(100 Hz) (Pa) | $G''$(100 Hz) (Pa) |
|---|---|---|---|---|---|
| 100% | 0.52 | 370 | 0.94 | 1.11 | 1.22 |
| 50% | 0.55 | 318 | 0.95 | 0.88 | 1.05 |
| 25% | 0.57 | 243 | 0.94 | 0.68 | 0.86 |
| 12.5% | 0.59 | 227 | 0.94 | 0.58 | 0.79 |
| 10% | 0.60 | 116 | 0.96 | 0.37 | 0.51 |
| 6.25% | 0.58 | 203 | 0.95 | 0.58 | 0.76 |
| 3.13% | 0.70 | 138 | 0.93 | 0.20 | 0.40 |
| 1.56% | 0.72 | 157 | 0.94 | 0.19 | 0.41 |
| 1% | 0.78 | 97 | 0.95 | 0.08 | 0.22 |
| 0.1% | 0.90 | 84 | 0.94 | 0.02 | 0.11 |

## DISCUSSION

In summary, we have determined with FCS the diffusive properties of nano-sized inert gold beads in the cytoplasm and the nucleus of living cells. HeLa, HepG2, and THLE cells showed a strong anomalous diffusion in both compartments, highlighting the crowded state of the respective compartments. Comparing THLE and HepG2 cells (both derived from liver tissue), the cancerous cell line (HepG2) consistently showed a larger residence time $\tau_s$ of the gold

particles in the confocal volume, i.e., a somewhat higher degree of crowding may be associated with the increased proliferation of cancer cells.

Having determined the diffusive properties, we quantified from that also the viscoelastic response of the cytoplasm and nucleoplasm in terms of the complex shear modulus $G(\omega)$. Both fluids displayed a strongly non-Newtonian character, highlighted by a power-law increase of the complex shear modulus $|G(\omega)| \sim \omega^{\alpha}$. The latter is associated with a power-law distribution of relaxation times within the fluid. Interestingly, the viscous and elastic contribution to $G(\omega)$ are of the same order of magnitude for high frequencies, i.e., the interior of cells has equally many facets of an elastic solid and a purely viscous liquid. Upon osmotic stress, the elastic contribution in $G(\omega)$ was seen to decrease and diffusion became more normal in the cytoplasm and the nucleus. Associated with this was a change in the scaling of $G(\omega)$, i.e., $\alpha$ changed from 0.53 to 0.66. Since in vitro experiments on artificially crowded fluids also showed a considerable reduction of $\alpha$ when the solvent was changed, the most likely explanation for this phenomenon is the reduction of entanglement among the proteins and the DNA enforced by a partial collapse/aggregation of the respective molecules due to poor solvent conditions. In fact, the Zimm model for polymer solutions/melts under varying solvent conditions yields a very good heuristic description of these experimental findings (cf. Eq. 3). The latter reasoning is supported by our observations for (diluted) frog egg extract and artificially crowded solutions with varying solvents.

Although the measured values of the degree of anomality $\alpha$ showed a Gaussian distribution in all cases, the residence times $\tau_s$ displayed an exponential to uniform distribution (Fig. 4). In fact, taking the Zimm model seriously, the (almost) exponential distribution $p(\tau_s)$ is consistent with the previous finding of an exponential distribution of masses in the cytoplasm (13). We also observed that the residence times $\tau_s$ had already increased at comparatively low concentrations of stress agents, whereas the anomality $\alpha$ had gone up only slightly. In terms of the Zimm model, this behavior may reflect that the intracellular conditions did not change abruptly from a good to a $\theta$ solvent (which changes $\alpha$, cf. Eq. 3), but rather there was a smooth transition with an initial increase in crowding (thus, a more hindered diffusion). Regarding the stress agents sucrose, raffinose, and NaCl, comparable concentrations induced the same effect on the measurements, although NaCl is twice as osmolar as sucrose due to its ionic composition. However, one has to take into account that NaCl may be taken up by the cells in higher amounts than sucrose because of its small molecular size, so that a direct comparison between the two stress agents does not seem appropriate.

Given the above observations and the surprisingly good and intuitive interpretation in terms of Eq. 3, it seems that viable cells try to keep their intracellular fluids in a state that resembles crowded polymer solutions under good solvent conditions. Upon introduction of strong osmotic stress, not only are the viscoelastic characteristics of the fluids strongly altered, but eventually the cell also undergoes apoptosis (39). One may speculate that cellular function relies on a certain crowding, i.e., the degree of crowding is evolutionarily conserved, as viscoelastic characteristics of intracellular fluids have also been reported for bacteria (15).

We would like to emphasize that the radius $R$ of the diffusing gold beads enters the above analysis in various (nontrivial) ways. Although $R$ appears directly in the denominator of Eq. 2, its impact is cancelled totally for normal diffusion via the Laplace-transformed MSD ($\tilde{v}$) due to the Einstein-Stokes equation ($\tilde{v} \sim k_B T/R$). It is conceivable, though, that $R$ enters Eq. 2 again in some way in the more general case of anomalous diffusion. It is also noteworthy that the effects of crowding (like the observed anomalous diffusion) always rely on comparable sizes of probe and ''crowder''. Thus, the radius $R$ will for certain influence the results as the crowding is tested on different scales. Although our gold beads were presumably inert due to incubation with bovine serum albumin and biotin (cf. Methods), we cannot rule out that intracellular proteins got stuck at the gold surface during the experiments. Since typical protein radii are $\sim$2 nm, the probe radius $R$ could have been roughly doubled in this way. However, given the above considerations, it seems safe to say that this uncertainty in radius may only slightly affect our results, e.g., by changing numbers in Table 1–3 by some factor of order unity.

We note, finally, that using FCS for assessing the viscoelasticity also has limitations. The temporal resolution is limited to times $>5$ $\mu$s, as on shorter timescales the photophysics of the fluorophore masks the diffusive contribution to the decay of the autocorrelation function. In the opposite case of large timescales, getting enough statistics for obtaining a reliable autocorrelation function becomes limiting, i.e., one is typically restricted to times $<1$ s. In our case, the reliable times were $5 \times 10^{-6}$ and $5 \times 10^{-1}$, i.e., a frequency range of approximately five orders of magnitude can be covered. Comparing this to previous approaches with single-particle tracking, FCS appears to be a convenient tool for determining the viscoelastic properties of complex fluids (even within living cells/tissues) on the mesoscopic level for a wide frequency range. Therefore, we are confident that FCS in combination with the theory proposed by Mason and Weitz (24) is a versatile tool to explore the viscoelastic properties of complex fluids on the nanoscale.

We thank T. Surrey for supplying us with *Xenopus* egg extract and K. Richter for help with the microinjector.

This work was supported by the Institute for Modeling and Simulation in the Biosciences in Heidelberg.

## REFERENCES

1. Fulton, A. 1982. How crowded is the cytoplasm *Cell.* 30:345–347.

2. Cremer, T., and C. Cremer. 2001. Chromosome territories, nuclear architecture and gene regulation in mammalian cells. *Nat. Rev. Genet.* 2:292–301.
3. Minton, A. 2001. The influence of macromolecular crowding and macromolecular confinement on biochemical reactions in physiological media. *J. Biol. Chem.* 276:10577–10580.
4. Hall, D., and A. Minton. 2003. Macromolecular crowding: qualitative and semiquantitative successes, quantitative challenges. *Biochim. Biophys. Acta.* 1649:127–139.
5. Ellis, R., and A. Minton. 2003. Cell biology: join the crowd. *Nature.* 425:27–28.
6. Ellis, R., and A. Minton. 2006. Protein aggregation in crowded environments. *Biol. Chem.* 387:485–497.
7. Luby-Phelps, K., D. Taylor, and F. Lanni. 1986. Probing the structure of cytoplasm. *J. Cell Biol.* 102:2015–2022.
8. Luby-Phelps, K., P. Castle, D. Taylor, and F. Lanni. 1987. Hindered diffusion of inert tracer particles in the cytoplasm of mouse 3T3 cells. *Proc. Natl. Acad. Sci. USA.* 84:4910–4913.
9. Seksek, O., J. Biwersi, and A. Verkman. 1997. Translational diffusion of macromolecule-sized solutes in cytoplasm and nucleus. *J. Cell Biol.* 138:131–142.
10. Arrio-Dupont, M., G. Foucault, M. Vacher, P. Devaux, and S. Cribier. 2000. Translational diffusion of globular proteins in the cytoplasm of cultured muscle cells. *Biophys. J.* 78:901–907.
11. Verkman, A. 2002. Solute and macromolecule diffusion in cellular aqueous compartments. *Trends Biochem. Sci.* 27:27–33.
12. Elsner, M., H. Hashimoto, J. Simpson, D. Cassel, T. Nilsson, and M. Weiss. 2003. Spatiotemporal dynamics of the COPI vesicle machinery. *EMBO Rep.* 4:1000–1004.
13. Weiss, M., M. Elsner, F. Kartberg, and T. Nilsson. 2004. Anomalous subdiffusion is a measure for cytoplasmic crowding in living cells. *Biophys. J.* 87:3518–3524.
14. Banks, D., and C. Fradin. 2005. Anomalous diffusion of proteins due to molecular crowding. *Biophys. J.* 89:2960–2971.
15. Golding, I., and E. Cox. 2006. Physical nature of bacterial cytoplasm. *Phys. Rev. Lett.* 96:098102.
16. Wachsmuth, M., W. Waldeck, and J. Langowski. 2000. Anomalous diffusion of fluorescent probes inside living cell nuclei investigated by spatially-resolved fluorescence correlation spectroscopy. *J. Mol. Biol.* 298: 677–689.
17. Schutz, G., H. Schindler, and T. Schmidt. 1997. Single-molecule microscopy on model membranes reveals anomalous diffusion. *Biophys. J.* 73: 1073–1080.
18. Weiss, M., H. Hashimoto, and T. Nilsson. 2003. Anomalous protein diffusion in living cells as seen by fluorescence correlation spectroscopy. *Biophys. J.* 84:4043–4052.
19. Saxton, M. 2002. Chemically limited reactions on a percolation cluster. *J. Chem. Phys.* 116:203–208.
20. Weiss, M. 2003. Stabilizing Turing patterns with subdiffusion in systems with low particle numbers. *Phys. Rev. E.* 68:036213.
21. Weiss, M., and T. Nilsson. 2004. In a mirror dimly: tracing the movements of molecules in living cells. *Trends Cell Biol.* 14:267–273.
22. Berry, H. 2002. Monte Carlo simulations of enzyme reactions in two dimensions: fractal kinetics and spatial segregation. *Biophys. J.* 83: 1891–1901.
23. Schnell, S., and T. Turner. 2004. Reaction kinetics in intracellular environments with macromolecular crowding: simulations and rate laws. *Prog. Biophys. Mol. Biol.* 85:235–260.
24. Mason, T., and D. Weitz. 1995. Optical measurements of frequency-dependent linear viscoelastic moduli of complex fluids. *Phys. Rev. Lett.* 74:1250–1253.
25. Janmey, P. 1991. A torsion pendulum for measurement of the viscoelasticity of biopolymers and its application to actin networks. *J. Biochem. Biophys. Methods.* 22:41–53.
26. Weiss, M., W. Welsch, M. von Schickfus, and S. Hunklinger. 1998. Viscoelastic behavior of antibody films on a shear horizontal acoustic surface wave sensor. *Anal. Chem.* 70:2881–2887.
27. Yamada, S., D. Wirtz, and S. Kuo. 2000. Mechanics of living cells measured by laser tracking microrheology. *Biophys. J.* 78:1736–1747.
28. Tseng, Y., J. Lee, T. Kole, I. Jiang, and D. Wirtz. 2004. Micro-organization and visco-elasticity of the interphase nucleus revealed by particle nanotracking. *J. Cell Sci.* 117:2159–2167.
29. Wong, I., M. Gardel, D. Reichman, E. Weeks, M. Valentine, A. Bausch, and D. Weitz. 2004. Anomalous diffusion probes microstructure dynamics of entangled F-actin networks. *Phys. Rev. Lett.* 92:178101.
30. Gardel, M., M. Valentine, J. Crocker, A. Bausch, and D. Weitz. 2003. Microrheology of entangled F-actin solutions. *Phys. Rev. Lett.* 91: 158302.
31. Bausch, A., W. Moller, and E. Sackmann. 1999. Measurement of local viscoelasticity and forces in living cells by magnetic tweezers. *Biophys. J.* 76:573–579.
32. Labhart, P. 1999. Ku-dependent nonhomologous DNA end joining in *Xenopus* egg extracts. *Mol. Cell. Biol.* 19:2585–2593.
33. Rigler, R. 2001. Fluorescence Correlation Spectroscopy. Springer Verlag, Berlin.
34. Hess, S., and W. Webb. 2002. Focal volume optics and experimental artifacts in confocal fluorescence correlation spectroscopy. *Biophys. J.* 83:2300–2317.
35. Saxton, M. 2001. Anomalous subdiffusion in fluorescence photobleaching recovery: a Monte Carlo study. *Biophys. J.* 81:2226–2240.
36. Hofling, F., T. Franosch, and E. Frey. 2006. Localization transition of the three-dimensional Lorentz model and continuum percolation. *Phys. Rev. Lett.* 96:165901.
37. Ferry, J. D. 1980. Viscoelastic Properties of Polymers. Wiley, New York.
38. Doi, M., and S. F. Edwards. 1986. The Theory of Polymer Dynamics. Oxford University Press, Oxford, UK.
39. Friis, M., C. Friborg, L. Schneider, M. Nielsen, I. Lambert, S. Christensen, and E. Hoffmann. 2005. Cell shrinkage as a signal to apoptosis in NIH 3T3 fibroblasts. *J. Physiol.* 567:427–443.